PERGAMON

International Journal of Heat and Mass Transfer 45 (2002) 877–889

International Journal of HEAT and MASS TRANSFER

www.elsevier.com/locate/ijhmt

Measurement of endwall heat transfer and pressure drop in a pin-fin wedge duct

Jenn-Jiang Hwang *, Chau-Chin Lui

Department of Mechanical Engineering, Chung-Hua University, Hsinchu 300, Taiwan, ROC

Received 15 March 2001

Abstract

This paper discusses the measurements of endwall heat transfer and pressure drop in a wedge-shaped duct inserted with an array of circular pin fins. The endwall surface is coated with a thin layer of thermochromic liquid crystals and a transient test is run to obtain detailed heat transfer distributions. Parametric studies include Reynolds number ($10,000 \leqslant Re \leqslant 50,000$), outlet flow orientation (straight and lateral) and pin configuration (staggered and in-line). The wedge duct has a convergent angle of 12.7°. The pin spacing-to-diameter ratios along the longitude and transverse directions are fixed at $s_x/d = s_y/d = 2.5$. Pin-less wedge duct results are also obtained for comparison. Results indicated that the straight wedge duct with a staggered pin array is most recommended because of its significant endwall heat transfer and moderate pressure-drop penalty; while the turned wedge duct with a staggered pin array is least recommended since it yields the highest pressure drops and raises severe hot spots. A similarity of the pin Reynolds-number dependence of row-averaged Nusselt number is developed in the present wedge duct of accelerating flow. © 2001 Published by Elsevier Science Ltd.

1. Introduction

Pin-fin arrays are commonly used to intensify internal heat transfer of a turbine blade or vane near the trailing section (Fig. 1). They also serve as a means to bridge the narrow span between the suction and pressure surfaces for structural purpose. Aerodynamic considerations demand a small wedge angle for the blade profile and, thus, the narrow channels in the trailing-edge region should be wedge cavities. In common cooling designs, the coolant from the blade bases either exits through the blade-tip slots or traverses the trapezoidal-shaped pin-fin channel and then is ejected from the slots along the edge of the airfoil [1]. Another cooling scheme employs coolant ejection through the trailing edge from the coolant cavity (Fig. 1). This would imply a main flow through a convergent pin-fin channel. The present experimental study is motivated by the need for a better understanding of the endwall heat transfer and pressure drop characteristics in a pin-fin wedge duct, which has not been studied previously.

VanFossen [2] conducted an experiment to examine the pin-length effect on the overall heat transfer coefficients in rectangular ducts with staggered pins, the results showed that short pins performed a better overall heat transfer than long pins. Metzger et al. [3] studied experimentally the local heat transfer variation in a rectangular duct with a staggered short pin array. They found that the local heat transfer increased in the first few rows, reached a peak value and then slowly decreased to a fully developed value. They developed the heat transfer correlations in terms of the Reynolds number for the staggered pin array. Then, Metzger and Haley [4] experimentally compared the endwall heat transfer to the overall pin array heat transfer in rectangular ducts inserted with a staggered pin array. They used wooden (thermally inactive) pins and calculated the heat transfer based on only the exposed endwall surface area. It was found that the endwall heat transfer coefficient had almost the same level as the combined pin-endwall average. Simoneau and VanFossen [5]

* Corresponding author. Tel.: +886-3537-4281x8334; fax: +886-3537-3771.

E-mail address: jjhwang@chu.edu.tw (J.-J. Hwang).

0017-9310/02/$ - see front matter © 2001 Published by Elsevier Science Ltd.
PII: S0017-9310(01)00193-4

Nomenclature

A_c	local cross-sectional area of the wedge duct (m^2)
A_{min}	local minimum cross-sectional area with pin blockage in the wedge duct (m^2)
c_p	specific heat at constant pressure (kJ kg^{-1} K^{-1})
D	equivalent hydraulic diameter at the wedge duct inlet (m)
d	pin diameter, Fig. 2 (m)
H_1	height of the entrance of the wedge duct, Fig. 2 (m)
H_2	height of the straight exit of the wedge duct, Fig. 2 (m)
h	heat transfer coefficient (kW m^{-2} K^{-1})
$\overline{h}$	area-averaged heat transfer coefficient (kW m^{-2} K^{-1})
K	pressure-drop coefficient ($= 2\Delta P/(\rho U^2)$)
k	thermal conductivity of the endwall material (W m^{-1} K^{-1})
k_f	air thermal conductivity (W m^{-1} K^{-1})
L	endwall length (along streamwise direction), Fig. 2 (m)
l	fin length (or height) (m)
$\overline{Nu}$	area-averaged Nusselt number based on the duct hydraulic diameter ($= \overline{h}D/k_f$)
$\overline{Nu}_d$	row-averaged pin Nusselt number on the endwall surface ($= \overline{h}d/k_f$)
$\overline{Nu}_s$	area-averaged Nusselt number for the pin-less duct
P_c	peripheral distance of the wedge duct (m)
ΔP	pressure drop across the test section (kPa)
Re	Reynolds number at the test duct inlet ($= \rho UD/\mu$)
Re_d	modified local Reynolds number ($= \rho U_{max} d/\mu$)
s_x	longitude spacing between the pins, Fig. 2 (m)
s_y	transverse spacing between the pins, Fig. 2 (m)
T_m	mainstream temperature (K)
T_i	initial wall temperature (K)
T_w	wall temperature (K)
t	transient test time (s)
U	bulk mean velocity at the duct inlet (m s^{-1})
U_{max}	mean velocity in the minimum flow area (m s^{-1})
W	width of the endwall plate, Fig. 2 (m)
X	streamwise coordinate, $X = 0$ at the sharp entrance of the duct, Fig. 2 (m)
x	streamwise coordinate with respect to the straight test section, Fig. 2 (m)
y	spanwise coordinate with respect to the straight test section, Fig. 2 (m)
z	distance normal to the bottom endwall (m)

Greek symbols

α	thermal diffusivity of the endwall material (m^2 s^{-1})
ρ	air density (kg m^{-3})
μ	viscosity of the air (kg s^{-1} m^{-1})
ϑ	wedge angle

Subscripts

b	bulk mean
d	pin
i	initial
m	mainstream
s	smooth
w	wall

performed an experimental work to examine the effect of array geometry and position on the heat transfer of an individual pin. The spanwise turbulence intensity profiles immediately upstream of the row containing the heated pin were also measured, the results showed the behavior of pin heat transfer bore a parallel to the development of the turbulence-intensity. Lau et al. [6] employed a mass transfer sublimating technique to measure the local endwall heat/mass transfer coefficients in rectangular channels with in-line and staggered pin arrays, the overall and row-averaged heat/mass transfer coefficients were compared well with the previous data [3]. Later, Lau et al. [7,8] further experimentally investigated the effect of lateral ejection on heat transfer and pressure drop characteristics in rectangular pin-fin channels. They demonstrated that, when air was allowed to eject through an array of small holes in one sidewall of a pin-fin channel, the decreasing rate of mass flow in the channel significantly affected the overall heat transfer from the channel and overall pressure drop across the channel. Baughn et al. [9] measured the local heat transfer coefficients on a pin-fin surface by two different isotherm-map methods namely, transient and heated-coating liquid crystal techniques, from which the values near the stagnant point of the pin fin were found to be compared fairly well. Chyu [10] used a mass transfer sublimating system to evaluate the effects of fillets at the cylinder-endwall junction and array geometry on the endwall heat transfer in rectangular ducts. Then, Chyu et al. [11] examined the pin-shape effect on the heat/mass transfer characteristics in a narrow rectangular channel. The staggered cube array was recommended due to its significant heat transfer enhancement and moderate pressure penalty. Recently, Hwang et al. [1] conducted an experiment to study the overall heat transfer and pressure drop characteristics in a pin-fin trapezoidal

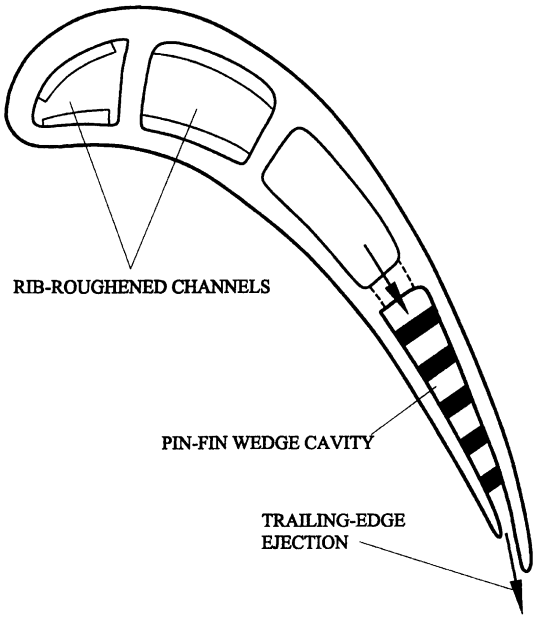

Fig. 1. Cross-sectional view of the modern internally cooled turbine blade.

duct with lateral ejection, the results revealed that the trapezoidal pin-fin duct with lateral outlet flow only has higher log-mean Nusselt numbers and pressure-drop coefficient than the straight counterpart.

As discussed, most of the prior work is restricted to flow normal to pin fins where the pin length keeps constantly along the streamwise direction. Strictly speaking, detailed heat transfer characteristics in a convergent pin-fin channel have not been reported yet. Hence, the objective of the present study is to investigate experimentally the endwall heat transfer and pressure drop characteristics in convergent pin-fin channels, which simulates the internal cooling cavities of the blade trailing edge. The effects of flow orientation, pin arrangement, and Reynolds number typical of the gas turbine application are examined. It is known that conventional thermal experimental methods are in general unable to provide data with a high degree of accuracy and fine grid for studies of local heat transfer on a surface over which there is a large variation in the heat transfer coefficient. Therefore, a transient liquid-crystal technique, similar to Ekkad and Han [12] and Hwang and Chen [13], is employed in the present study to measure the local heat transfer on the endwall surfaces. This transient technique not only is a full-surface measurement in characteristic but also can be applied to complex geometry [9]. Moreover, the complicated work in quantifying the heat losses during the steady-state heat transfer experiments is not required. The detailed distributions of heat transfer coefficient that are provided by the present work could afford a better understanding of the endwall heat transfer enhanced by pin fins in a wedge channel. They could also provide a reference for computational-fluid-dynamic-based studies as relating to the pin-fin heat transfer in a convergent channel.

2. Experiments

2.1. Apparatus

The experimental apparatus, shown schematically in Fig. 2, consists of a blowing-type flow circuit, the test section and a computer-based image-processing system. A 5-hp centrifugal blower blows the outdoor air into the flow circuit. The air passes through a flow meter that measures the volumetric flow rate of air and then enters an electric heater to be heated to a required temperature.

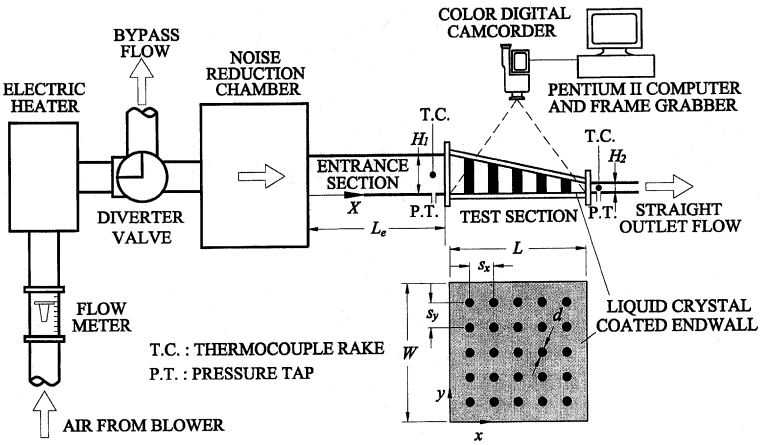

Fig. 2. Schematic drawing of the experimental apparatus and the test section.

The hot air from the heater subsequently traverses a noise-reduction chamber, an entrance section, and then flows into the test section. Finally, the air exits either laterally or from the straight outlet (Fig. 3) to the outside of building via an exhaust system. The wedge-shaped test section and the cylindrical pins are made of Plexiglas®. The bottom endwall of a square area of 160 mm × 160 mm ($L \times W$) is sprayed with liquid crystals, representing the heat transfer active surface (the shaded region in Fig. 3). Twenty-five circular pins of diameter $d = 12.0$ mm span the distance between two principal duct walls. All pins stand vertically on the bottom endwall. They have different lengths from $l/d = 1.3$ to 3.6 depending on the location within the wedge duct. The pin spacings along the longitude and transverse directions are the same, i.e., $s_x = s_y = 30.0$ mm. The heights of the duct entrance (H_1) and straight exit (H_2) are 48.0 and 12.0 mm, respectively, forming a wedge angle of about 12.7°. To investigate the effect of the outlet flow orientation, either the straight exit or the lateral exit is blocked by a Plexiglas® blockage. The blockage is screwed from the top and bottom walls of the channel rather than being attached permanently to the test section. As shown in Fig. 2, two thermocouple rakes (each has five beads) are located at the test-section entrance and exit (straight or lateral), respectively, to measure the mainstream temperatures. A real-time hybrid recorder (YOKOGAWA, AR 1100A) records the time-dependent mainstream temperatures. In addition, nine pressure taps are installed at the entrance and two exits of the test section (each has three taps) for the static-pressure measurement. They are connected to a transmitter (MODUS) to display the pressure-drop signals.

The image-processing system, as shown in Fig. 2, includes a digital color camcorder (SONY DCR-TRV7) and a frame grabber interface associated with a Pentium II personal computer. The camcorder is focused on the liquid-crystal-coated surfaces to view and record their color change during the transient test. The frame grabber interface is programmed to analyze the color changes using image-processing software. The software analyzes the picture frame-by-frame and simultaneously records the time lapse of the liquid crystals from colorless to green during the transient test.

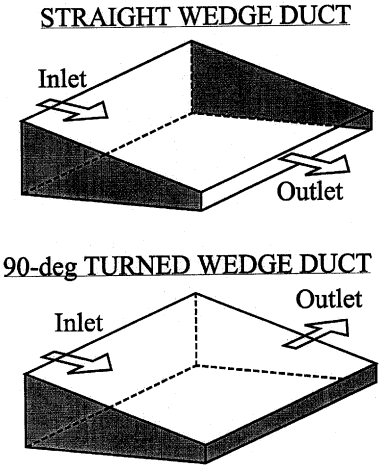

Fig. 3. Two wedge ducts of different orientations of outlet flow.

As shown in Fig. 3, two wedge ducts of different outlet-flow orientations are tested. The first one has a straight outlet flow, which simulates the internal cooling system that the coolant is provided from the coolant cavity, traverses the convergent pin-fin duct, and then ejects from the trailing-edge slots. In the second wedge duct, the main flow turns laterally, exits from the trapezoidal cross-section outlet, and then exits from flow blade-tip slots. Each duct is inserted with in-line or staggered pins (not an equilateral triangular array).

The endwall surface is sprayed with black background paints and then liquid crystals (Hallcrest, BW/R38C5W/C17-10). These coatings are light sprays of thickness of the order of 10 μm. The test section is assembled and sealed from air leakage with petroleum jelly. The camcorder is set up and focused on the endwall surface.

2.2. Experimental procedure

Transient test of the heat transfer measurement is carried out by suddenly exposing the hot air to the test section, which results in a color change of the surface coatings. The liquid crystals are colorless at room temperature. These then change to red, green, blue and finally colorless again during the heating process. The color change temperatures to red, green and blue are 38.2, 39.0 and 43.5 °C, respectively [13].

Before the test run, the hot air bypasses the test section so that the endwall remains at the laboratory ambient temperature. The flow is kept in diversion until the required mainstream temperature has been achieved, typically at about 60–70 °C. Then, the valve turns to route the hot air into the test section and, simultaneously, the recorder is switched on to record the mainstream temperature history. The image-processing system records the transition time for the color change to green, and transfers the data into a matrix of time of the color change over the entire surface. The time and temperature data are transferred into a computer program to obtain the local heat transfer coefficient.

2.3. Data analysis and uncertainty

The local heat transfer coefficient over the test surface can be obtained by assuming one-dimensional transient conduction over a semi-infinite solid, for which

the initial condition and boundary conditions on the liquid crystal coated surface are

$$k\frac{\partial^2 T}{\partial z^2} = \rho c_p \frac{\partial T}{\partial t} \tag{1}$$

as $t = 0, \quad T = T_i; \qquad$ as $t > 0,$

$$k\frac{\partial T}{\partial z} = h(T_w - T_m) \quad \text{at } z = 0; \qquad T = T_i \quad \text{as } z \to \infty.$$

The surface temperature response is shown as

$$\frac{T_w - T_i}{T_m - T_i} = 1 - \exp\left(\frac{h^2\alpha t}{k^2}\right)\operatorname{erfc}\left(\frac{h\sqrt{\alpha t}}{k}\right). \tag{2}$$

The heat transfer coefficient h can be calculated by knowing the wall temperature (T_w), the initial surface temperature (T_i), the oncoming mainstream temperature (T_m), and the corresponding time (t) required to change the coated-surface color to green at any location. The time required for the color change in a typical run is about 15–90 s depending on the location, mainstream temperature and duct throughflow rate. This testing time is so short that the heat flow can hardly penetrate the depth of the Plexiglas® plate, so as to ensure the validity of the assumption of the semi-infinite solid on the test surface.

Since T_m is time-dependent, the solution of Eq. (2) should be modified: first, the mainstream temperature history is simulated as a series of time step changes. Then, the time step changes of the mainstream temperature are included in the solution for the heat transfer coefficient using Duhamel's superposition theorem. The solution at every location is therefore represented as

$$T_w - T_i = \sum_{j=1}^{n}\left\{1 - \exp\left[\frac{h^2\alpha(t-\tau_j)}{k^2}\right] \times \operatorname{erfc}\left[\frac{h\sqrt{\alpha(t-\tau_j)}}{k}\right]\right\}\left[\Delta T_{m(j,j-1)}\right], \tag{3}$$

where $\Delta T_{m(j,j-1)}$ and τ_j are the temperature and time step changes obtained from the recorder output.

Two kinds of Reynolds numbers are discussed herein to examine their effects on the heat transfer and pressure drop characteristics in smooth and pin-fin wedge ducts: One is based on the mean velocity and the equivalent hydraulic diameter at the wedge duct entrance, i.e.,

$$Re = \rho U D/\mu. \tag{4a}$$

This indicates the hydrodynamic state of mainflow approaching the wedge duct with and without pin arrays and is similar to that in VanFossen [2]. The other one is based on the superficial maximum velocity in the pin-fin wedge and the pin diameter and is expressed as

$$Re_d = \rho U_{max} d/\mu. \tag{4b}$$

This has been widely used in many pin-fin heat transfer studies, for example, Metzger et al. [3,14] and Lau et al. [7,8]. Note that since increasing row number decreases the minimum cross-sectional area in the present pin-fin wedge duct, Re_d is dependent on the axial location. For distinction, Re and Re_d are referred to "duct Reynolds number" and "pin Reynolds number", respectively, in the following discussion.

Similar to the Reynolds-number definition, the non-dimensional heat transfer coefficients on endwall surfaces are represented by "duct Nusselt number" and "pin Nusselt number", respectively, as

$$\overline{Nu} = \overline{h}D/k_f, \tag{5a}$$

$$\overline{Nu}_d = \overline{h}d/k_f. \tag{5b}$$

The pressure drop across the finite-length duct of wedge cross-section, either with straight or with lateral outlets, can be made dimensionlessly [15] as

$$K = 2\Delta P/(\rho U^2). \tag{6}$$

The pressure-drop coefficient obtained is based on adiabatic conditions (i.e., test with ambient-temperature mainstream).

By the method of Kline and McClintock [16], the estimated maximum uncertainties of the investigated parameters are as follows: h, 7.9%; Re, 6.4%; Re_d, 6.8%; and K, 7.7%. The individual contributions to the uncertainties of the above parameters for each of the measured physical properties are summarized in Table 1.

3. Results and discussion

3.1. Smooth duct results

Before the subsequent discussion of the results in pin-fin wedge ducts, it is very important to determine the heat transfer and pressure-drop coefficients in a pin-less wedge duct to understand the isolated effect of flow acceleration. In addition, these smooth wedge duct results can further provide a base to obtain the extent of heat-transfer augmentation and pressure-loss penalty by pin fins in a wedge duct.

A comparison of the area-averaged Nusselt number between the smooth wedge and rectangular ducts is made in Fig. 4(a). Airflow is introduced from an upstream plenum through a sharp-edge inlet into the test duct, and transient-liquid-crystal measurements of the heat transfer coefficient are conducted on the bottom surfaces between $2.2 \leqslant X/D \leqslant 4.4$. The previous correlation (dashed line, [17]) for fully developed flow in a circular pipe is also plotted for comparison. Note that the Nusselt numbers for the wedge and rectangular ducts are based on the same characteristic length (i.e., hydraulic diameter at the duct entrance, Eqs. (4a) and

Table 1
Typical nondimensional interval for the relevant variables

Variables	Uncertainty
Equivalent duct hydraulic diameter, D	±0.5%
Specific heat of air, c_p	±3.0%
Kinetic viscosity of air, μ	±2.9%
Wall thermal diffusivity and conductivity, α and k	±0%
Time of color change, Δt	±1.0%
Main stream temperature, T_m	±3.0%
Air density, ρ	±1.6%
Air mass flux, G	±5.4%
Pressure difference, ΔP	±5.1%

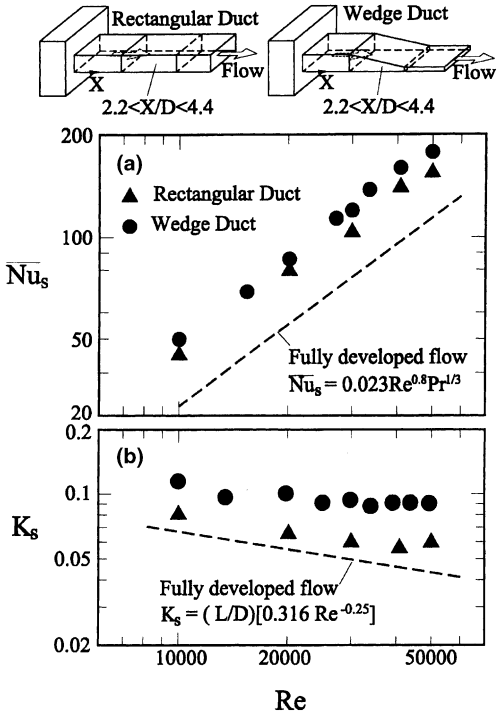

Fig. 4. Comparison of the length-mean heat transfer and pressure-drop coefficients of the straight wedge and rectangular pin-less ducts.

(4b)), such that these data can really reflect the flow acceleration effect in the wedge duct. It is evident that the increase in heat transfer due to the flow acceleration effect is about 10–20%. In addition, owing to the entrance effect, the Nusselt numbers in the present two ducts are higher than those for the fully developed values in a circular pipe, typically about 40–60%. The percentage increase in heat transfer due to the entrance effect is quantitatively consistent with the previously published data [18], for which the axial location of three diameters from a sharp-edge inlet has an entrance effect of about 56%. Fig. 4(b) shows the pressure drops across the straight wedge and rectangular ducts as a function of the duct Reynolds number. The dashed line represents Mill's results [19] of the fully developed flow. It is seen that, due to the flow acceleration effect, the pressure-drop coefficient of the wedge duct is higher than that of the rectangular duct, and is subsequently higher than the previous correlation for the fully developed flow due to the entrance effect. The agreement with the comparison is satisfactory, such that the data obtained by the present experiments are reliable.

3.2. Detailed heat transfer coefficient distributions

Typical examples for the detailed heat transfer coefficient distributions on the endwall surfaces of pin-fin ducts are shown in Figs. 5–7.

As shown in Fig. 5, the heat transfer in the region immediately ahead and alongside of every pin, both for the wedge and rectangular ducts, is very similar to that near a single cylinder [20]. In these regions, the values of h are relatively high and the local maxima exist. In the rectangular duct (Fig. 5(b)), the trend of h increases initially in the first two rows to reach a maximum at the second row and then followed by a subsequent decline between the third and fifth rows, similar to that observed by Chyu [10]. In contrast, the heat transfer coefficients on the endwall surfaces of the wedge duct (Fig. 5(a)) increase with increasing row number due to the flow acceleration effect.

Figs. 6(a) and (b) show the Reynolds-number effect on local heat transfer distributions on the endwall surface of the straight wedge duct with an in-line pin array. An increase in Re increases the heat transfer coefficients, and the sidewall effects of the wedge duct are clearly seen from the relatively low heat transfer coefficients near the upper and lower sides. A comparison between Fig. 6(b) and (c) illustrates the effect of pin arrangement under a fixed Reynolds number ($Re = 20{,}000$). For an in-line pin array (Fig. 6(b)), the flow through the spanwise spacing between neighboring pins is roughly similar to flow in a straight channel. The span interac-

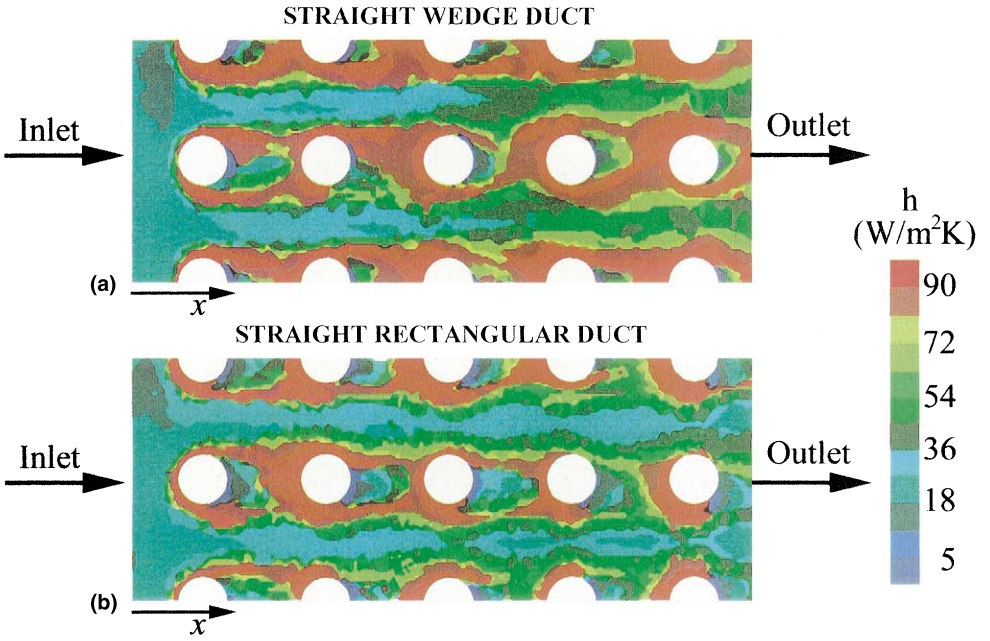

Fig. 5. Detailed heat transfer coefficient distributions around the mid-column on the endwall of the (a) straight wedge duct and (b) the straight rectangular duct with an in-line pin array, $Re = 16{,}800$.

tions within the array in such a throughflow are therefore weak. In contrast, the local heat transfer coefficient distribution in Fig. 6(c) seems to be more uniform and slightly higher. This is because the staggered pin array induces a significant shedding-wake effect which causes a flow interaction in both streamwise and spanwise directions. In general, the effect of pin arrangement on the heat transfer coefficient distribution in the present convergent duct is similar to that in the channel of identical cross-sectional area [21].

The effect of outlet-flow orientation on heat transfer distributions is illustrated by comparing Figs. 6(b) and 7(a). Obviously, the distribution of local heat transfer is significantly altered as the outlet flow is turned from the straight exit to the lateral exit. Physically, the duct convergence retards the straight flow; thus, most of the fluid turns laterally immediately after entering the wedge duct, and then exits from the relatively large open close to the duct inlet. This results in a significant heat transfer enhancement on the endwall surfaces around the upper-left quarter of the plot ($0 \leqslant x/L \leqslant 0.5$ and $0.5 \leqslant y/W \leqslant 1.0$). However, a large portion of endwall surface near the corner formed by the sidewall and the blocked straight exit ($0.8 \leqslant x/L \leqslant 1.0$ and $0 \leqslant y/W \leqslant 0.2$) can hardly sense the mainflow, and so, the heat transfer is degraded considerably. The pin-arrangement effect on the local heat transfer distributions on the endwall surfaces is shown in Fig. 7(a) and (b). In the turned wedge duct, the pin arrangement seems to insignificantly affect the local heat transfer. For these two cases, the mainflow has to turn to the lateral exit totally; in such a way, both the pin arrays appear to be in a staggered fashion to the turning flow. Therefore, with respect to the turning main flow, the pin arrangements are largely alike. Even so, the hot spots near the blocked straight exit ($x/L = 1.0$) become severe for the staggered pin array since they balk the straight flow to impinge the blocked straight exit.

3.3. Area-averaged endwall heat transfer

Fig. 8 shows the area-averaged endwall Nusselt number as a function of the duct Reynolds number for the pin-fin wedge ducts investigated. The dash-dotted line represents the present results of the smooth wedge duct of straight flow. As shown in Fig. 8, in the straight wedge ducts, the staggered pin array has a higher endwall-averaged heat transfer than the in-line pin array. As mentioned above, the staggered pin array produces more tortuous flow than does the in-line pin array, and hence, enhances heat transfer. The previous study of a rectangular pin-fin duct [10] revealed a similar trend. As for the 90° turned wedge ducts, the endwall-averaged heat transfer is nearly independent of the pin arrangements investigated. This can be clearly seen from the distributions of local heat transfer coefficients in Fig. 7. Quantitatively, the area-averaged endwall heat transfer is degraded about 15% and 30%, respectively, for the

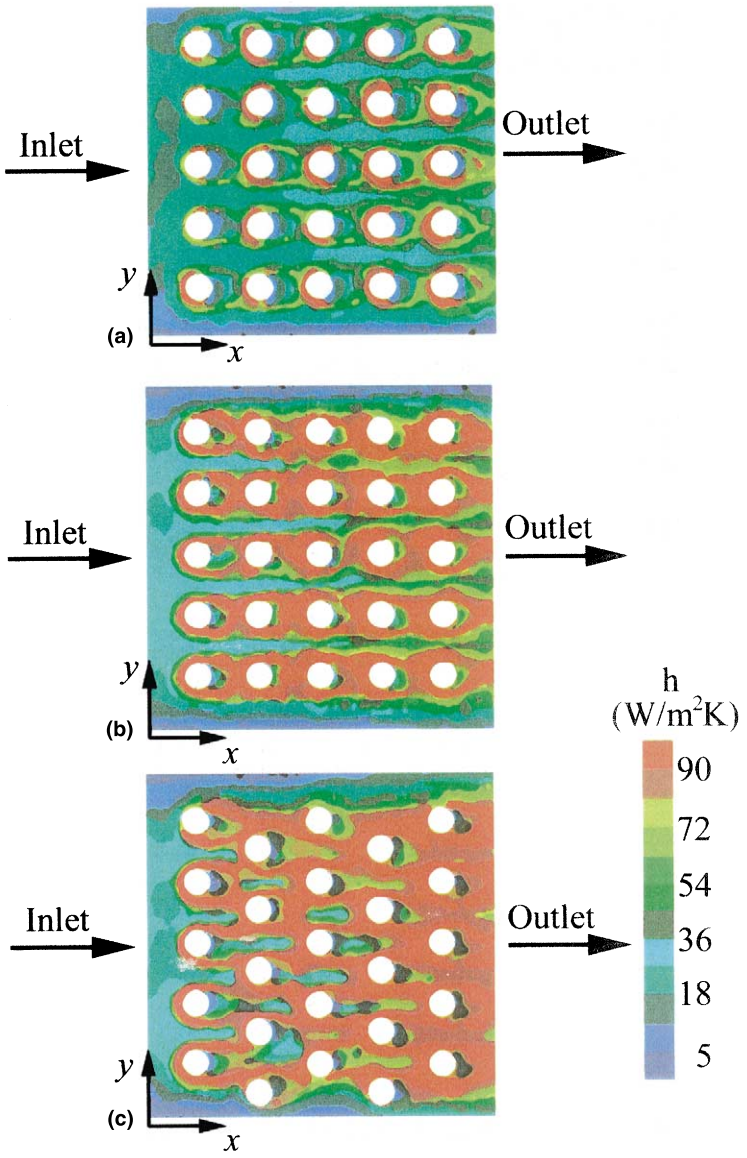

Fig. 6. Detailed heat transfer coefficient distributions on the endwall surfaces of the straight wedge ducts (a) in-line pin array, $Re = 10{,}000$, (b) in-line pin array, $Re = 10{,}000$, and (c) staggered pin array, $Re = 20{,}000$.

in-line and staggered pin arrays as the flow turns laterally from the straight exit. Hence, for the heat transfer coefficient, the straight pin-fin wedge duct is preferable to the pin-fin turned wedge duct. The previous study of a rectangular pin-fin duct [7] reached the same conclusion, but the trapezoidal-duct results by Hwang et al. [1] revealed an opposite tendency. The higher heat transfer for the lateral ejection than the straight flow in the trapezoidal duct is owing the effect of flow acceleration through a convergent lateral exit for the trapezoidal duct, which does not occur in the present wedge duct and the previous rectangular duct.

Fig. 8 further shows the least-square curvefit lines of the present experiments. They can be represented as the forms of

$$\overline{Nu} = C_1 Re\, C_2. \qquad (7\text{-}1)\text{–}(7\text{-}3)$$

The values of C_1 and C_2 for the four ducts investigated are listed in Table 2. Note that the data of the 90° turned duct with staggered and in-line pin arrays are almost the same and can be therefore put into a single equation. The maximum deviation between the equations above and the experimental data shown in Fig. 8 is less than 8.8%.

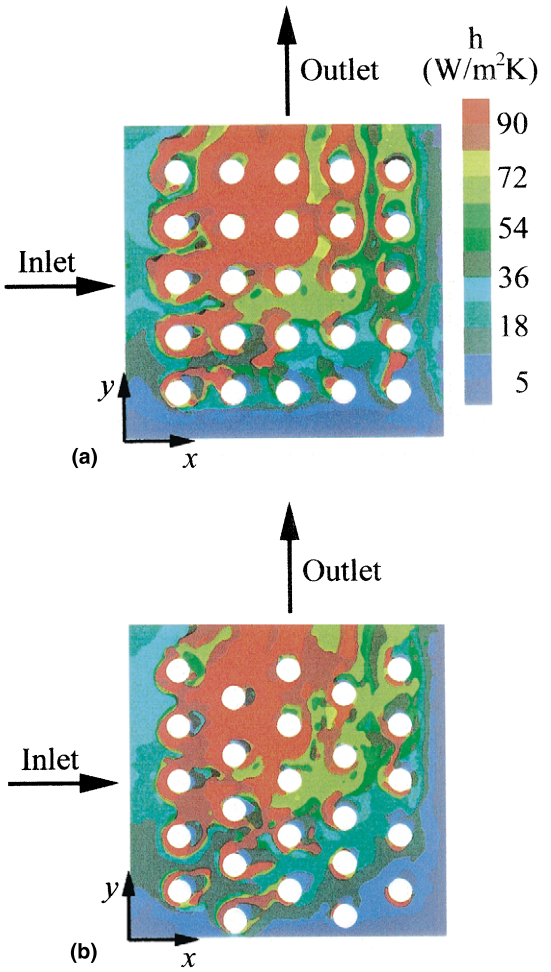

Fig. 7. Detailed heat transfer coefficient distributions on the endwall surfaces of the turned wedge ducts (a) in-line pin array, $Re = 20{,}000$, and (b) staggered pin array, $Re = 20{,}000$.

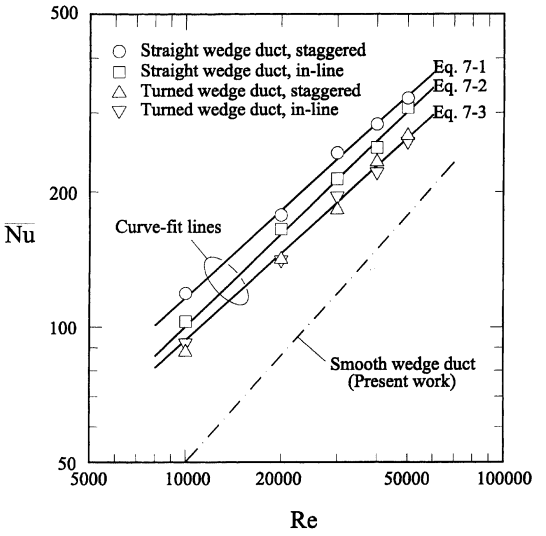

Fig. 8. Area-averaged endwall Nusselt number as a function of the duct Reynolds number.

3.4. Correlation for row-averaged Nusselt number

According to the previous studies [3,10] and the data shown in Fig. 5(b), the maximum row-resolved Nusselt number occurs at the second row for the in-line arrays in a narrow rectangular channel. In contrast to this general trend, the heat transfer coefficient in the present straight wedge ducts shown in Fig. 5(a) increases monotonically with the increase of row number due to the flow acceleration effect. It is very important to know the relation of the row-averaged heat transfer between the accelerating flow in the present wedge duct and the uniform flow in the rectangular duct. The effect of local through flow velocity on the row-averaged Nusselt number is examined in the present accelerating-flow duct. For a given channel and array geometry, as the volume flow rate in the straight wedge duct is maintained the same, the pin Reynolds number shown in Eq. (5a) and (5b) can be expressed as

$$Re_{\mathrm{d}} = Re \frac{\tan\vartheta}{H_1 - x\tan\vartheta} \frac{A_{\mathrm{c}}}{A_{\min}} \frac{d}{D_{\mathrm{in}}}, \tag{8}$$

where ϑ is the wedge angle, $A_{\min}$ is the local minimum cross-sectional area with pin blockage, and A_{c} is the local unobstructed wedge duct cross-sectional area. Both $A_{\min}$ and A_{c} are x dependent. For a fixed pin spacing, however, the area ratio $A_{\mathrm{c}}/A_{\min}$ is kept constant, and therefore, the pin Reynolds number increases with increasing axial distance. Figs. 9 and 10 show the row-

Table 2
Coefficients of heat transfer correlations

Duct flow orientation	Pin configuration	$\overline{Nu} = C_1 Re C_2$			
		C_1	C_2	Deviation	Equation
Straight	Staggered	0.289	0.651	3.9%	(7-1)
Straight	In-line	0.168	0.692	5.1%	(7-2)
90° turned	Staggered and in-line	0.259	0.640	8.8%	(7-3)

averaged Nusselt number ($\overline{Nu}_d$) as a function of the local pin Reynolds number (Re_d). Since the heat transfer in the first row has a distinctive feature compared to the downstream rows [10], their data are displayed in Fig. 10 individually. The present data shown in these two figures are averaged over the mid-three pin columns for each row. Some previous correlations for array-averaged Nusselt number in pin-fin ducts are plotted in these two figures and are further listed in Table 3 for comparison. Both works have rectangular ducts of a fixed pin height ($l/d = 1.0$), and their pin spacings ($s_x/d = s_y/d = 2.5$) are the same as those in the present work. In general, the array-averaged data can represent the corresponding fully developed values [10]. It is seen from Fig. 9 that the present row-averaged Nusselt numbers increase with increasing pin Reynolds number for both the staggered and in-line pin arrays. Interestingly, the data seem to be row-number independent, indicating that there is a similarity of Re_d-dependence of $\overline{Nu}_d$ for different pin rows in the present wedge duct. In addition, the data spread along the fully developed rectangular-duct correlations almost. This means that both these rectangular-duct correlations can, to a certain extent, represent the present row-resolved data in the wedge duct. A correlation of the present data is developed in the form of

$$\overline{Nu}_d = 0.145\,Re_d^{0.646}. \tag{9}$$

The maximum deviation between the present experimental data and the prediction from Eq. (9) is less than 7.8%. As for the in-line pin array (Fig. 9), the present data compare fairly well with Chyu's correlation (Table 3). The above discussion suggests a similarity of the Re_d-dependence of $\overline{Nu}_d$ between the accelerating flow in the present pin-fin wedge ducts and the fully developed flow in the previous pin-fin rectangular ducts.

As for the first-row data (Fig. 10), the trend is quite similar to that in Fig. 9 for the downstream row data. The data are independent of pin arrangement and can be correlated as

$$\overline{Nu}_d = 0.125\,Re_d^{0.651}. \tag{10}$$

The maximum deviation between the present experimental data and that predicted from Eq. (10) is less than 6%. Also, the previous correlations for rectangular pin-fin ducts give a satisfactory representation of the present data in a wedge pin-fin duct.

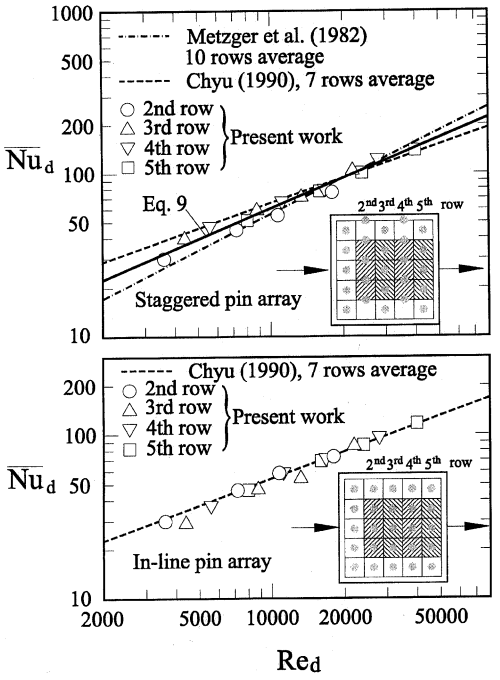

Fig. 9. Row-averaged Nusselt number as a function of the pin Reynolds number for the second to fifth pin rows.

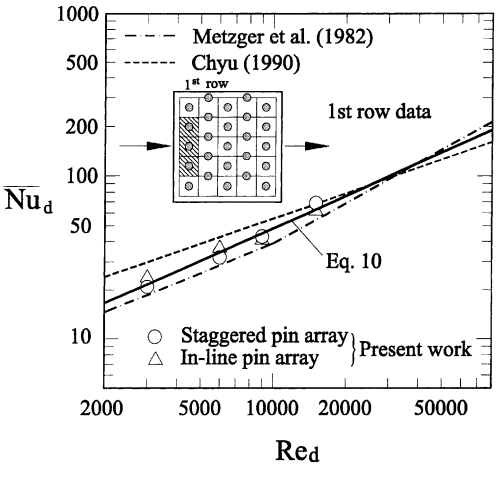

Fig. 10. Row-averaged Nusselt number as a function of the pin Reynolds number for the first pin row.

3.5. Pressure-drop coefficients

Fig. 11 depicts the pressure-drop coefficient (K) for the pin-fin wedge ducts as a function of the duct Reynolds number (Re). The present results of straight pinless wedge ducts (dashed line) are also included for comparison. As shown in Fig. 11, the pressure drop for the straight wedge duct with a staggered pin array is higher than that with an in-line pin array, and subsequently higher than that across the pin-less wedge duct. Compared to the pin-less results, the increase in pressure drop due to the staggered and in-line pin arrays is about 2.0–2.8 and 3.4–4.5 times, respectively. As for the flow turns laterally, the pressure drops are significantly aug-

Table 3
Comparison of the present row-averaged correlations in the wedge duct and the previous array-averaged correlations in the rectangular duct

Studies	Staggered	In-line	The first row
Metzger et al. [3]	$\overline{Nu}_d = 0.069\,Re_d^{0.782}$	–	$\overline{Nu}_d = 0.140\,Re_d^{0.611}$ $(1000 \leqslant Re_d \leqslant 10{,}000)$
			$\overline{Nu}_d = 0.022\,Re_d^{0.831}$ $(10{,}000 \leqslant Re_d \leqslant 100{,}000)$
Chyu [10]	$\overline{Nu}_d = 0.598\,Re_d^{0.511}$	$\overline{Nu}_d = 0.401\,Re_d^{0.537}$	$\overline{Nu}_d = 0.330\,Re_d^{0.550}$
Present work	$\overline{Nu}_d = 0.145\,Re_d^{0646}$	$\overline{Nu}_d = 0.401\,Re_d^{0.537}$	$\overline{Nu}_d = 0.125\,Re_d^{0.651}$

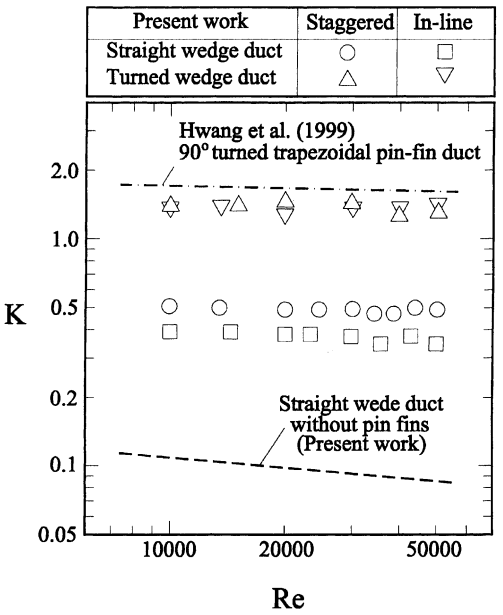

Fig. 11. Reynolds-number dependence of the pressure-drop coefficient of the pin-fin wedge ducts.

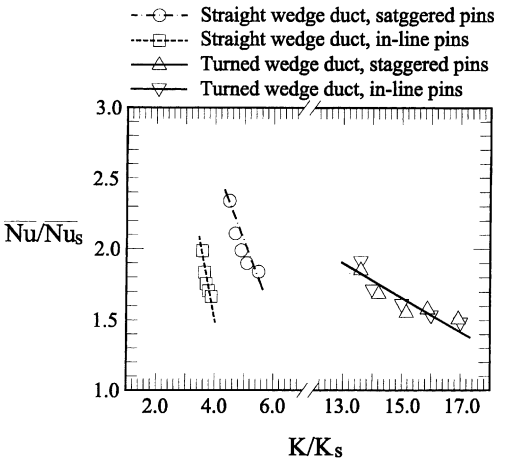

Fig. 12. Relation between the heat-transfer augmentation and pressure-drop penalty in the present wedge ducts.

mented, typically about 13–17 times that of the straight pin-less wedge duct. This is because the duct with lateral outlet flow produces a separated flow near the concave corner formed by the sidewall and the blocked straight exit. In addition, the swirling secondary flow that occurs due to the imbalance of the centripetal forces is a result of the curvature of the duct centerline. Both these effects increase the pressure drop between the duct entrance and exit. Note that the pressure drops across the turned wedge ducts with in-line and staggered pin arrays are almost the same, and both do not differ from those in the 90° turned trapezoidal pin-fin duct [1] (dash-dotted line, shown in Fig. 11) too much.

3.6. Performance consideration

Fig. 12 illustrates the relation between the endwall-averaged heat transfer enhancement and pressure-drop penalty in the pin-fin wedge duct investigated. Both heat transfer and pressure loss coefficients are normalized by the present results of the straight pin-less wedge duct (Fig. 5). A notable trend revealed in Fig. 12 is that the heat transfer enhancement $\overline{Nu}/\overline{Nu}_s$ generally decreases with an increase in K/K_s. Such a decreasing trend is most significant for the straight wedge duct with a staggered pin array and much less for the turned wedge pin-fin ducts. In sum, the straight wedge duct with a staggered pin array appears to be one of the most attractive configurations since it produces the highest endwall heat transfer enhancement with moderate pressure-drop penalty. However, the turned wedge duct with a staggered pin array is least recommended due to its largest pressure-drop penalty as well as the existence of severe hot spots.

4. Concluding remarks

An experimental study has been performed to investigate the endwall heat transfer coefficients and overall pressure drops in converging ducts inserted with various-length pin fins, as to simulate the trailing edge cooling cavities of turbine blades. The effects of

outlet flow orientation, pin-fin configuration, and flow Reynolds number are examined. The major contributions are as follows: first, we provided new information of detailed heat transfer distributions on the endwall surfaces of convergent pin-fin channels of different outlet flow orientations. Then, we developed a similarity of the pin Reynolds-number dependence of row-averaged Nusselt number in the present pin-fin wedge duct of accelerating flow, which can reduce much of the tedious effort in correlating the data for the wedge duct of parametric variations. We find thereby:

1. In the straight wedge duct, the heat transfer coefficients on the endwall surfaces increase with increasing row number due to the flow acceleration effect. This trend is different from that in a rectangular duct with uniform pin length.
2. In the straight wedge duct, owing to the stronger flow interaction in both streamwise and spanwise directions, the staggered pin array produces relatively uniform and higher local heat transfer distribution than does the in-line pin array. In the 90° turned wedge duct, however, the local heat transfer coefficient distributions are not affected too much by the pin arrangement. They are significantly enhanced near the lateral exit but are largely deteriorated near the remote corner formed by the sidewall and the blocked straight exit.
3. In the straight wedge duct, the staggered pin array produces about 15% higher endwall-averaged heat transfer than the in-line pin array. Turning the outlet flow laterally from the straight exit reduces the endwall-averaged heat transfer about 15% and 30% for the staggered and in-line pin arrays, respectively.
4. With respect to the local pin Reynolds number, there is a similarity between the row-averaged Nusselt number in the present pin-fin wedge duct and the array-averaged Nusselt number in the previous pin-fin rectangular duct.
5. In the straight wedge duct, the staggered pin array pays more pressure-drop penalty than the in-line pin array, typically about 4.4–5.5 and 3.2–3.8 times the pin-less wedge duct, respectively. In the wedge duct with a lateral exit, the pressure drops across the in-line and staggered pin arrays are almost the same, typically about 13.5–17 times the straight pin-less wedge duct.
6. The straight wedge duct with a staggered pin array is most recommended since it produces the highest endwall heat transfer enhancement with moderate pressure-drop penalty. Contrarily, the turned wedge duct with a staggered pin array pays the highest pressure-drop penalty as well as raises severe hot spots and, thus, is least recommended.

Acknowledgements

This work is sponsored by the National Science Council and Taiwan Power Company under contract of NSC 87-TPC-E-216-002.

References

[1] J.J. Hwang, D.Y. Lai, Y.P. Tsia, Heat transfer and pressure drop in pin-fin trapezoidal ducts, Trans. ASME J. Turbomach. 21 (1999) 264–272.
[2] G.J. VanFossen, Heat-transfer coefficients for staggered arrays of short pin fins, Trans. ASME J. Heat Transfer 104 (1982) 268–274.
[3] D.E. Metzger, R.A. Berry, J.P. Bronson, Developing heat transfer in rectangular ducts with staggered pin fins, Trans. ASME J. Heat Transfer 104 (1982) 700–706.
[4] D.E. Metzger, S.W. Haley, Heat transfer experiments and flow visualization for arrays of short pin fins, ASME Paper No. 82-GT-138, 1982.
[5] R.J. Simoneau, G.J. VanFossen, Effect of location in an array on heat transfer to short cylinder in crossflow, Trans. ASME J. Heat Transfer 106 (1984) 42–48.
[6] S.C. Lau, Y.S. Kim, J.C. Han, Local endwall heat/mass transfer distributions in pin fin channels, AIAA J. Thermophys. Heat Transfer 1 (1987) 365–372.
[7] S.C. Lau, J.C. Han, Y.S. Kim, Turbulent heat transfer and friction in pin fin channels with lateral flow injection, Trans. ASME J. Heat Transfer 111 (1989a) 51–58.
[8] S.C. Lau, J.C. Han, T. Batten, Heat transfer, pressure drop, and mass flow rate in pin fin channels with long and short trailing edge ejection holes, Trans. ASME J. Turbomach. 111 (1989) 116–123.
[9] J.W. Baughn, P.T. Ireland, T.V. Jones, N. Saniei, A comparison of the transient and heated-coating methods for the measurement of local heat transfer coefficients on a pin fin, Trans. ASME J. Heat Transfer 111 (1989) 877–881.
[10] M.K. Chyu, Heat transfer and pressure drop for short pin-fin arrays with pin-endwall fillet, Trans. ASME J. Heat Transfer 112 (1990) 926–932.
[11] M.K. Chyu, Y.C. Hsing, V. Natarajan, Convective heat transfer of cubic fin arrays in a narrow channel, Trans. ASME J. Turbomach. 120 (1998) 362–367.
[12] S.V. Ekkad, J.C. Han, Local heat transfer distributions near a sharp turn of a two-pass smooth square channel using a transient liquid crystal image technique, J. Flow Visual. Image Process. 2 (1995) 285–297.
[13] J.J. Hwang, C.S. Chen, Augmented heat transfer in a triangular duct by using multiple swirling jets, Trans. ASME J. Heat Transfer 121 (1999) 683–690.
[14] D.E. Metzger, C.S. Fan, S.W. Haley, Effects of pin shape and array orientation on heat transfer and pressure loss in pin fin arrays, Trans. ASME J. Heat Transfer 106 (1984) 252–257.
[15] J.J. Hwang, Turbulent heat transfer and fluid flow a porous-baffled channel, AIAA J. Thermophys. Heat Transfer 11 (1997) 429–436.

[16] S.J. Kline, F.A. McClintock, Describing uncertainties on singlesample experiments, Mech. Eng. 75 (1953) 3–8.
[17] F.W. Dittus, L.M.K. Boelter, University of California at Berkeley, Publ. Eng. 2 (1930) 443.
[18] W.M. Kays, M.E. Crawford, Convective Heat and Mass Transfer, McGraw-Hill, New York, 1980.
[19] A.F. Mills, in: D. Richard (Ed.), Basic Heat and Mass Transfer, Irwin, MA, 1995.
[20] R.J. Goldstein, M.K. Chyu, R.C. Hanin, Measurement of local mass transfer on a surfaces in the region of the base of portruding cylinder with computer-controlled data acquisition system, Int. J. Heat Mass Transfer 28 (1985) 977–985.
[21] M.K. Chyu, R.J. Goldstein, Influence of cylindrical elements on local mass transfer from a flat surface, Int. J. Heat Mass Transfer 34 (1991) 2175–2186.